1550 nm range high-speed single-mode vertical-cavity surface-emitting lasers

© S.A. Blokhin[1], A.V. Babichev[2], L.Ya. Karachinsky[2], I.I. Novikov[2], A.A. Blokhin[1], M.A. Bobrov[1], A.G. Kuzmenkov[1], N.A. Maleev[1], V.V. Andryushkin[2], V.E. Bougrov[2], A.G. Gladyshev[3], D.V. Denisov[4], K.O. Voropaev[5], I.O. Zhumaeva[5], V.M. Ustinov[6], H. Li[7], S.C. Tian[8,9], S.Y. Han[8,9], G.A. Sapunov[8,9], A.Yu. Egorov[3,10], D. Bimberg[8,9]

[1] Ioffe Institute,
194021 St. Petersburg, Russia
[2] ITMO University,
197101 St. Petersburg, Russia
[3] Connector Optics LLC,
194292 St. Petersburg, Russia
[4] St. Petersburg State Electrotechnical University „LETI",
197022 St. Petersburg, Russia
[5] OAO OKB-Planeta,",
173004 Veliky Novgorod, Russia
[6] Submicron Heterostructures for Microelectronics, Research and Engineering Center, Russian Academy of Sciences,
194021 St. Petersburg, Russia
[7] College of Mathematical and Physical Sciences, Qingdao University of Science and Technology,
266061 Qingdao, China
[8] Bimberg Chinese-German Center for Green Photonics, Changchun Institute of Optics,
Fine Mechanics and Physics (CIOMP), Chinese Academy of Sciences (CAS),
130033 Changchun, China
[9] Center of Nanophotonics, Institute of Solid State Physics, Technische Universität Berlin,
10623 Berlin, Germany
[10] Alferov Federal State Budgetary Institution of Higher Education and Science Saint Petersburg
National Research Academic University of the Russian Academy of Sciences,
194021 St. Petersburg, Russia

E-mail: blokh@mail.ioffe.ru

Received May 17, 2022
Revised June 16, 2022
Accepted June 16, 2022

The results of complex studies of static and dynamic performance of 1550 nm-range VCSELs, which were created by direct bonding (wafer fusion technique) InAlGaAs/InP optical cavity wafers with AlGaAs/GaAs distributed Bragg reflector wafers grown by molecular beam epitaxy, are presented. The VCSELs with a buried tunnel junction diameter less than 7 μm demonstrated a single-mode lasing with a side-mode suppression ratio more than 40 dB; however, at diameters less than 5 μm, a sharp increase in the threshold current is observed. It is associated to the appearance of a saturable absorber due to penetration of optical mode into the non-pumped regions of the active region. The maximum single-mode output optical power and the -3 dB modulation bandwidth reached 4.5 mW and 8 GHz, respectively, at 20°C. The maximum data rate at 20°C under non-return-to-zero on-off keying modulation was 23 Gb/s for a short-reach link based on single-mode fiber SMF-28. As the length of the optical link increased up to 2000 m, the maximum data rate dropped to 18 Gbit/s. The main factors affecting the high-speed operation and data transmission range are defined and discussed, and the further ways to overcome themit are proposed.

Keywords: VCSEL, wafer fusion, molecular beam epitaxy, single-mode operation, high-speed performance.

DOI: 10.21883/SC.2022.08.54120.9890

1. Introduction

The demands of the data centers and the supercomputers growing yearly to increase the traffic-carrying capacity and, at the same time, the length of the optical interconnections stimulate not only the active introduction of the communication optical lines based on the single-mode fiber, but search in new technical solutions as well. Due to the low energy consumption, the low losses in the SM fibers and compatibility with the classic technology of wavelength division multiplexing, there is an evident round of scientific interest in the vertical-cavity surface-emitting lasers (VCSEL) [1]. As the traffic-carrying capacity of the communication optical channels can be increased within the technology of the spatial division multiplexing (SDM) using the few-mode fiber (FMF) or the multicore fiber (MCF) [2], using the VCSELs for implementation of the new-generation multi-channel optical data transmission is a

very promising solution [3]. At the same time, the long-wave VCSELs open wide perspectives in implementation of low-cost and energy-efficient high-speed multi-channel long optical interconnections [4]. Thus, the increase in the speed and range of the optical data transmission using the single-mode long-wave VCSELs is utterly relevant.

The classical method of creating the monolithic (i.e. grown in a single growth process) 1550 nm-range VCSELs based on the system of the InAlGaAsP/InP materials is associated with a problem of low contrast of the refraction indices and low heat conductivity of the ternary and quaternary InP lattice-matched solid solutions, thereby resulting to the strong self-heating effect and limiting the output optical power (~ 1.6 mW @ 20°C) and the high-speed performance (~ 4 GHz @ 20°C) [5]. The alternative method of creation of the 1550 nm-range VCSELs is a combination of the active range based on the system of the InAlGaAsP/InP materials with the distributed Bragg reflectors (DBR) simultaneously having a high reflectivity and increased heat conductivity. Presently, there are two main promising approaches: the hybrid integration of the optical resonator with high-contrast metal-dielectric mirrors (hereinafter referred to as HC-VCSEL) and the wafer fusion technology (hereinafter referred to as WF-VCSEL).

Within the first approach, the replacement of only one semiconductor InAlGaAs/InAlAs DBR with the dielectric mirror has resulted in the increase in the modulation bandwidth of the HC-VCSEL with the active region based on the strained InAlGaAs quantum wells (QW) up to 12 GHz at 25°C [6] and demonstrated a back-to-back data transmission (BTB) at the speed of up to 25 Gbit/s with direct current modulation in the nonreturn-to-zero mode (NRZ) [7]. Due to application of the concept of the short-cavity and reduction of a diameter of the current aperture, this approach has been further developed to implement record-high small-signal modualtion bandwidth ~ 22 GHz @ 25°C and to increase the data transmission rate to 50 Gbit/s in the BTB configuration, as well as to demonstrate faultless data transmittivity via the single-mode fiber SMF-28 for 200 m at 40 Gbit/a and 1 km at 28 Gbit/s without applying the algorithms of digital predistortion and error correction [8]. However, the approach used in the HC-VCSEL design based on minimization of the mode volume in order to achieve higher resonance frequencies significantly limits the output optical power of the lasers [9]. The disadvantages of the described approach also include the necessity of using special dielectric materials (AlF_3, ZnS, CaF_2) for DBR formation.

The second approach can unify unique possibilities of the system of the InAlGaAsP/InP materials (in terms of implementation of the effective active region) with the advantages of the system of the AlGaAs/GaAs materials (in terms of creation of the effective semiconductor DBRs) to obtain the record-high (> 6 mW @ 20°C) output power in the single-mode lasing [10,11] without applying the additional methods of selection of the high-order modes in contrast to the first approach [12]. It should be noted that despite the necessity of subsequent double fusion of the wafer of the InAlGaAsP/InP optical resonator with the wafers of the upper and lower AlGaAs/GaAs DBR, the WF-VCSELs of this kind potentially can ensure the reliability that satisfies to the standard GR-468-CORE Telcordia [13]. In case of application of the InAlGaAs quantum wells as the active region, the maximum modulation bandwidth around 8 GHz has been achieved and the error-free data transmission for 10 km at 10 Gbit/s has been demonstrated in the NRZ-modulation mode [14]. For further improvement of the laser high-speed performance we have proposed to used the active region based on the thin strained InGaAs/InAlGaAs quantum wells [15]. In terms of implementation of sharp heterointerfaces, the most preferable option is to apply the molecular beam epitaxy (MBE) technology as it ensures growth control atomically in contrast to the metallo-organic chemical vapor deposition (MOCVD) [16]. Recently, we have shown the general applicability of the MBE method at all the stages of VCSEL heterostructure creation, including the epitaxial re-growth for formation of the buried tunnel junction (BTJ) [17] and demonstrated the effective WF-VCSELs of the spectral range of 1300 nm [18,19].

The study presents the results of the detailed VCSEL studies of the spectrum range of 1550 nm realized within the MBE method and the wafer fusion technology. The statical characteristics and the mode composition of the laser radiation are studied depending on the size of the current aperture. The method of the small-signal frequency analysis has been applied to investigate the mechanisms limiting the high-speed performance of the lasers. It has included determination of the range of optical data transmission using the developed single-mode lasers at the direct current modulation in the NRZ-mode.

2. Experimental samples

The WF-VCSEL was designed with the geometry of the vertical optical microresonator surrounded by undoped semiconductor DBRs, with injection of the carriers through the intracavity contact layers (IC layers) of the *n*-type and the tunnel junction for minimization of absorption at the free carriers [10,11]. The WF-VCSEL hybrid heterostructure (Fig. 1) of the spectrum range of 1550 nm is formed by subsequent double fusion of the wafer of the optical InAlGaAs/InP resonator with the wafers of the upper DBR based on the 22.5 pairs of the AlGaAs/GaAs layers and the lower DBR based on the 35.5 pairs of the AlGaAs/GaAs layers on the Wafer Bonding System EVG 510. The specifics of the technology applied for wafer fusion are given in the study [20]. The active region was the strongly-strained $In_{0.74}Ga_{0.26}As$ QWs of the thickness of 2.4 nm (the lattice mismatch parameter $\sim 1.4\%$), separated by the lattice-matched barrier $In_{0.53}Al_{0.16}Ga_{0.31}As$ layers. In order to increase the mode amplification by modification of the longitudinal confinement factor, the number of the wells is increased to 10, while the thickness of the

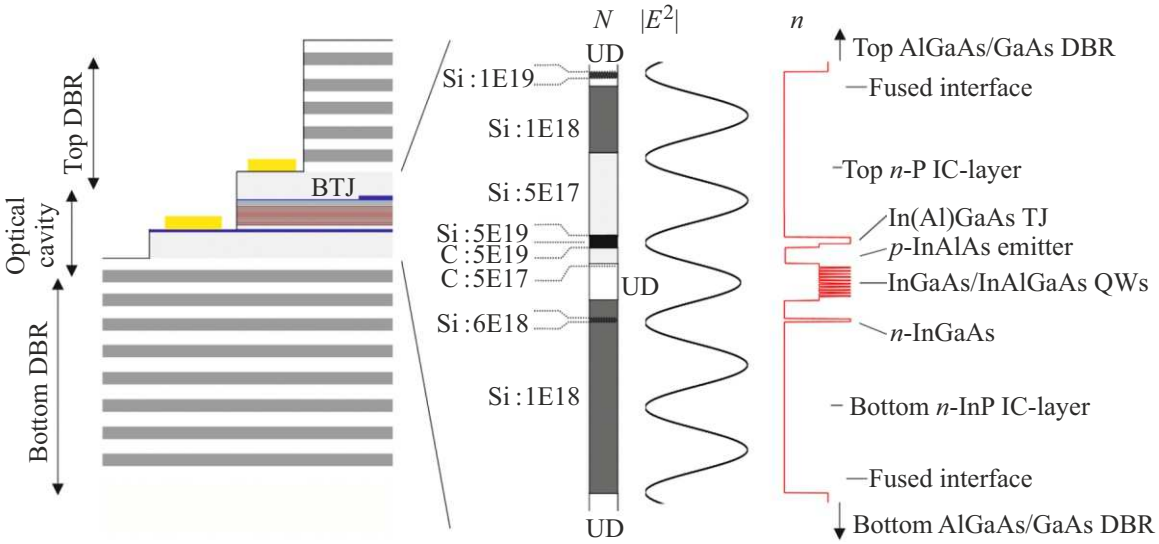

Figure 1. Schematic presentation of the transverse section of the device design of the WF-VCSEL and the distribution of the intensity of the fundamental mode electromagnetic field $|E^2|$ (in relative units) and the doping level N (in cm^{-3}) along the refraction index profile n within the microresonator. DBR — the distributed Bragg reflector, IC — the intracavity contact, TJ — the tunnel, BTJ — the buried tunnel junction, QW — the quantum well, UD — undoped.

barriers is decreased to 7 nm [15]. As a result, the total strain of the layers of the active region was $\sim 0.36\%$ in relation to the InP substrate material. The lateral current and optical confinements were realized in within the BTJ concept [21] by formation in the composite $In_{0.53}Ga_{0.47}As/In_{0.53}Al_{0.16}Ga_{0.31}As$ of the tunnel junctions of small mesas of the diameter of $4-8\,\mu$m by chemical etching of the n^{++}- and p^{++}-$In_{0.53}Ga_{0.47}As$ layers with subsequent epitaxial re-growth of the surface relief by the n-InP layer with the modulated doping profile [17]. The mesa etching depth was selected as a compromise between the high output optical power in the single-mode lasing and suppression of the effect of the saturating absorber in the non-pumped parts of the active region, which occurs in a relatively weak transverse optical confinement [22]. It should be noted that the epitaxial growth of the initial heterostructures of the optical resonator and the DBRs as well as the burial process have been implemented by the MBE method on the industrial unit Riber 49. Other details of the WF-VCSEL heterostructure design are given in the studies [17,22].

The device design of the WF-VCSEL is a triple mesa structure (Fig. 1) fabricated as follows. The first mesa is formed by plasma-chemical etching in the inductively-coupled plasma in the upper AlGaAs/GaAs DBR for opening up the upper IC layer. The second mesa is formed by chemical etching in the InAlGaAs/InP optical resonator for opening up the lower IC layer. The third mesa is formed by chemical etching in the lower IC layer in order to reduce the capacitance of contact pads. The SiN dielectric layer is formed by plasma-chemical deposition for electrical insulation. The windows to the contact layers are formed by plasma-chemical etching of the SiN dielectric. The contacts and the contact pads Ti/Pt/Au are formed by the lift-off method. The special features for manufacturing of the lasers of this type are given in the study [23].

3. Results and discussion

Fig. 2 shows the current-voltage and watt-ampere characteristics (WAC) for WF-VCSELs with a various diameter of the BTJ mesa diameter, which are measured within the wide range of the temperatures. The lasers with the BTJ mesa diameter of $4\,\mu$m exhibit a jump-like increase in the output optical power with the increase in the pumping current, accompanied by the sharp increase in the observed value of the threshold current (hereinafter referred to as WAC nonlinearity), thereby impeding adequate evaluation of the slope efficiency of the lasers (see Fig. 2, *a*). As this VCSEL design is not optimized for operation at high levels of dissipated power, the thermal WAC rollover is observed at relatively small operating currents ~ 13 mA, thereby limiting the maximum output optical power at the level of 3.4 mW. The devices exhibit the lasing via the fundamental mode (the so-called single-mode regime) with the side mode suppression ratio (SMSR) > 50 dB within the whole operating range of the pumping currents (see Fig. 3, *a*). The observed WAC nonlinearity can be caused by both the sharp increase in the diffraction losses at the BTJ mesa periphery [24] as well as by the formation of the saturating absorber outside the BTJ mesa region (taking into account the lateral current spreading) [25]. The increase in the external temperature of the laser results in amplification of the WAC nonlinearity effect and lasing disappearance at the temperatures $> 40^\circ$C. As the light

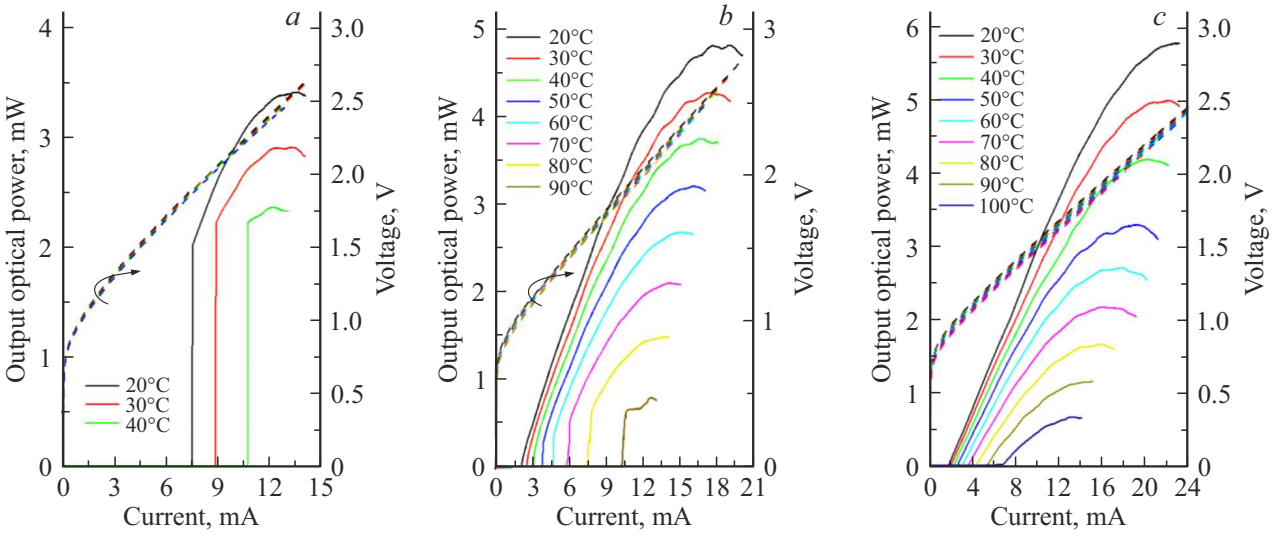

Figure 2. Current-voltage characteristics and watt-ampere characteristics of WF-VCSEL with the BTJ mesa diameter 4 (a), 6 (b) and 8 μm (c).

scattering/diffraction on the refraction index heterogeneities weakly depends on the external temperature, it can be suggested that it is mainly contributed by the light absorption at the resonance wavelength in the unpumped parts of the active region, which is sharply amplifying as the maximum of the amplification spectrum of the active region approaches the resonance wavelength of the microresonator.

With the increase in the BTJ mesa size, there is attenuation of the WAC nonlinear effect and the increase in the limit temperature, at which the lasing is observed, which is caused by a growing transverse confinement factor for the fundamental mode. Thus, the lasers with the BTJ mesa diameter 6 μm exhibit the lasing with the threshold current < 2 mA and the slope efficiency 0.4 W/A at the temperature of 20°C. The differential resistance does not exceed 95–100 Ohm due to omitting the InGaAsP layers as the contact layers. Since the VCSEL thermal resistance is reversely proportional to the size of the current aperture, and the series electrical resistance is reversely proportional to the area of the current aperture, then the self-heating effect with the current increase is mostly pronounced in the lasers with the small sizes of the current aperture. The increase in the BTJ mesa size can extend the range of the operating currents and increase the maximum output optical power to 4.8 mW (see Fig. 2, b). The limit value of the wall-plug efficiency is up to 20%. It should be noted that the increase in the lateral sized of the buried relief (regrowtth of the surface relief formed in the TJ) results in the reduction of the transverse confinement factor for the high-order modes and contributes to the implementation of the single-mode lasing with high sizes of the BTJ mesa. As a result, the lasers demonstrate stable single-mode operation with the magnitude SMSR > 45 dB at the BTJ mesa size below 7 μm.

With the increase in the temperature to 70°C, there is evidently the increase in the threshold current to 6 mA as well as the fall of the maximum output optical power and wall-plug efficiency to 2.1 mW and 9%, respectively. The limit temperature at which the lasing is observed is up to 95°C. It should be noted that at the temperatures > 50°C, specific features inherent to the effect of the saturating absorber, which is related to reduction of the actual spectral mismatch of the resonance wavelength of the microresonator in relation to the gain spectrum of the active region with the increase in the temperature.

For the lasers with BTJ mesa size > 7 μm, the WAC nonlinear effect is fully suppressed (the transverse confinement factor is close to 100%). However, there is anomalous WAC behaviour of another kind — the increase in the slope efficiency with the increase in the pumping current. Thus, the lasers with the BTJ mesa size of 8 μm at the temperature of 20°C exhibit the lasing with the threshold current < 2 mA, the wall-plug efficiency $\sim 19\%$ and the maximum output optical power of ~ 5.8 mW (see Fig. 2, c). At the small pumping currents, the slope efficiency reaches 0.35 W/A (the region I), but at the higher currents it increases to 0.41 W/A (the region II). This effect may be related to specific features of the change of the mode composition of lasing emission. The analysis of the lasing spectra has revealed a sharp fall of the magnitude SMSR and switching into the multi-mode lasing within the region II (see Fig. 3, c). Apparently, the detected behavior is related to irregularity of distribution of the pumping current density across the area (the current concentration at the BTJ mesa periphery, the so-called current crowding), which is typical for VCSEL with carrier injection through the IC layers [26] and leading to the reduction of the effective injection of the charge carriers for the fundamental mode in comparison with the high-order modes. It should be noted that the

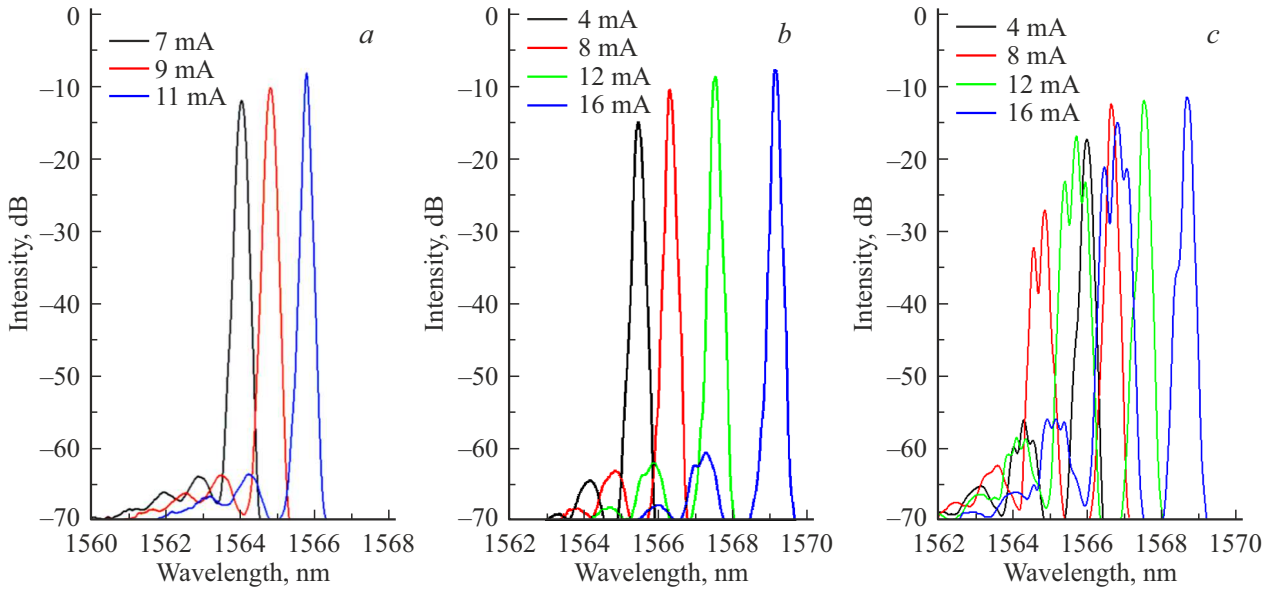

Figure 3. WF-VCSEL lasing spectra with the BTJ mesa diameter 4 (a), 6 (b) and 8 μm (c), measured at the temperature of 20°C.

detected effect will be amplified with further increase in the BTJ mesa size.

With the increase in the temperature, there is evidently a growing threshold current, predominantly caused by the thermal escape of the carriers from the thin InGaAs quantum wells [11]. Thus, at the temperature 70°C, the threshold current increases to 3.5 mA, and the maximum output optical power and the wall-plug efficiency fall to 2.2 mW and 9.5%, respectively. The limit temperature at which the lasing is observed is up to $\sim$ 110°C. Moreover, the WAC inflection point between the regions I and II is shifted towards the bigger currents, while the difference in the slope efficiency is negated, which is apparently related to the sharp increase in the optical losses for the high order modes in the unpumped parts of the active region.

It should be noted that the previously realized single-mode WF-VCSELs of the spectrum range of 1550 nm based on the InGaAs quantum wells and the n^+/p^+-InAlGaAs tunnel junctions have demonstrated the smaller efficiency ($\sim$ 14%) despite the higher slope efficiency, which is apparently related to the higher electric resistance of the devices and the smaller number of the quantum wells [11]. At the same time, the 1550 nm-range single-mode WF-VCSELs based on the InAlGaAs quantum wells and with the n^+/p^+-InAlGaAs tunnel junctins are much inferior in terms of the threshold current values with the comparable level of the slope efficiency [10,14]. At the same time, the 1550 nm-range HC-VCSELs based on the InAlGaAs quantum wells and with the n^+-InGaAs/p^+-InAlGaAs tunnel junctions in the geometry of the short microresonator demonstrate the single-mode lasing only at the BTJ mesa sizes $< 5\,\mu$m, thereby limiting the maximum output optical power at the level of 2.2 mW [9].

The small-signal frequency analysis (measurement of the S-parameters) was performed using the vector circuit analyzer Rodhe & Schwarz ZVA 40 and the photodetector New Focus 1434 with the bandpass 25 GHz. The high-speed performance of the injection laser in the current modulation mode is affected by thermal effects which limit the attainable resonance frequency, damping of the relaxation oscillations resulting in the reduction of the resonance peak amplitude, and by a bandpass (the cutoff parasitic frequency) of the electrical circuit connecting the signal generator and the internal source of the laser oscillations therebetween. However, the strong effect of the saturating absorber, which is usually accompanied by the hysteresis impedes adequate interpretation of the dynamic characteristics of the lasers with the BTJ diameter $< 5\,\mu$m. Fig. 4, a shows the amplitude-frequency characteristics (AFC, the parameter S_{21}) for the lasers with the BTJ diameter of 6 μm which are measured at the temperature of 20°C. The effective modulation bandwidth $f_{-3\,\mathrm{dB}}$ (evaluated by the AFC fall level at -3 dB) reaches 6 GHz at the pumping current of 4.5 mA and then is saturated at the level of $\sim$ 8 GHz. The corresponding value of the MCEF-factor ($\mathrm{MCEF} = f_{-3\,\mathrm{dB}}/(I - I_{th})^{0.5}$), determining the modulation current efficiency factor (MCEF) stays within the range $\sim 3.6\,\mathrm{GHz/mA}^{0.5}$. The obtained results correlate well with the data for the 1550 nm-range WF-VCSELs based on the InAlGaAs quantum wells and the n^+/p^+-InAlGaAs tunnel junctions [14].

In order to evaluate the WF-VCSEL key parameters, the classical model of response of the single-frequency laser to the sinusoidal modulation of the pumping current has been applied [27]. In order to minimize the error when solving the reverse problem of measurement data analysis S_{21}, the cutoff parasitic frequency of the low-frequency

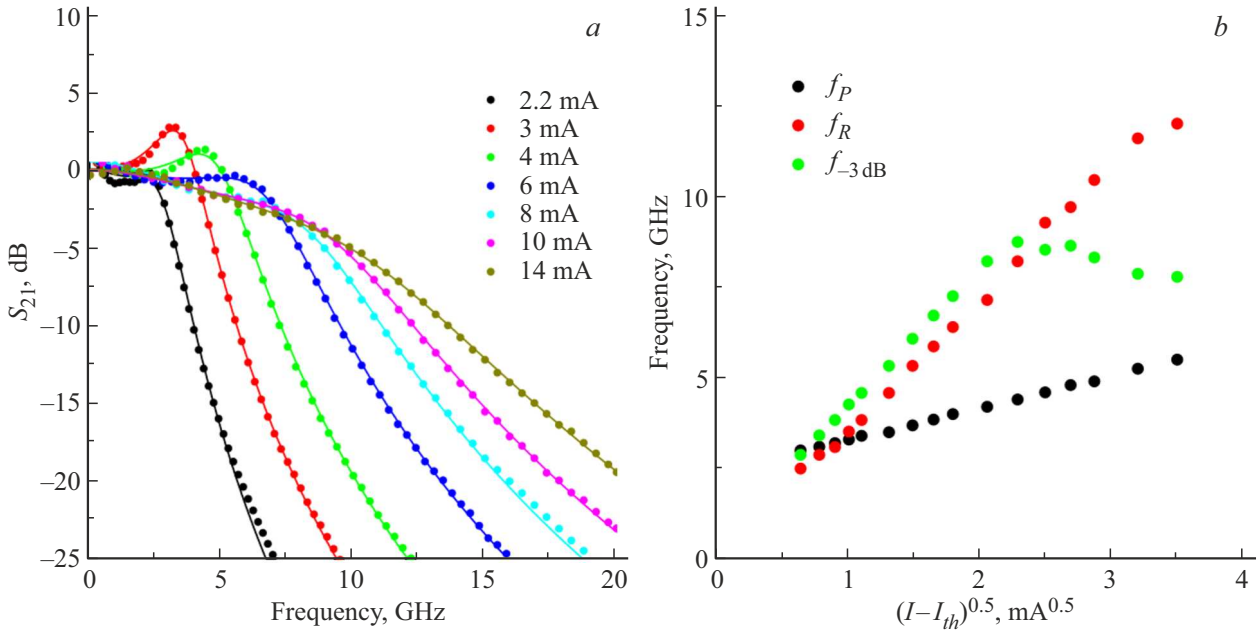

Figure 4. Results of the WF-VCSEL low-signal frequency analysis with the BTJ diameter of 6 μm: *a*) the amplitude-frequency characteristics S_{21} at the various current; *b*) the dependences of the cutoff parasitic frequency f_P, the resonance frequency f_R and the -3 dB modulation bandwidth $f_{-3\,\mathrm{dB}}$ on the current. The measurement temperature — 20°C.

filter formed by the electric elements of the laser has been independently determined from the equivalent laser diagram rebuilt based on the data of measurement of the reflectance of the input HF-signal (the parameter S_{11}). According to the results of Fig. 4, *b*, the cutoff parasitic frequency f_P of the laser with the BTJ diameter 6 μm is first of all growing with the pumping current, but at the voltages > 1.6 V it is saturated at the level of ~ 5 GHz. The rate of rise of the resonance frequency with the current, the so-called D-factor ($D = f_R/(I - I_{th})^{0.5}$), which reflects the level of the differential gain and the mode volume, exceeds 3.2 GHz/mA$^{0.5}$, which is noticeably higher than results obtained for the 1550 nm-range WF-VCSELs based on the InGaAs quantum wells and the n^+/p^+-InAlGaAs tunnel junctions [11]. As a result, the resonance frequency f_R at the pumping currents > 6 mA exceeds the effective modulation frequency and reaches ~ 12 GHz.

The obtained values indicate a substantial potential of the proposed active region. In fact, in accordance with the analysis of the main mechanisms affecting the high-speed performance of VCSELs, with domination of the thermal effects, the maximum modulation bandwidth is determined by the resonance frequency, and in accordance with the expression $f_{-3\,\mathrm{dB,thermal}} = \sqrt{1+\sqrt{2}}f_R$, it reaches ~ 18 GHz, thereby substantially increasing the experimental values $f_{-3\,\mathrm{dB}}$. In case of the domination of the mechanism related to the low cutoff parasitic frequency, the maximum modulation bandwidth, in accordance with the expression $f_{-3\,\mathrm{dB,parasitics}} = (2+\sqrt{3})f_P$, provides the value > 18 GHz. With domination of the effect of damping of the relaxation oscillations, the maximum modulation bandwidth is determined by the rate rise of the damping coefficient with the square of the resonance frequency, the so-called *K*-factor, and, in accordance with the expression $f_{-3\,\mathrm{dB,damping}} = 2\pi\sqrt{2}/K$, it exceeds 20 GHz at the moderate densities of the photons (the corresponding value $K \sim 0.45$ ns). Thus, the combination of the two last mechanisms leads to the sharp decrease in the amplitude of the resonance peak at the relatively small pumping currents.

It should be noted that the value of the cutoff parasitic frequency is mainly contributed by the parasitic capacitance of the region of the reversely shifted p^+n-transition (outside the BTJ), so with the increase in the BTJ mesa size, some increase in the frequency f_P is observed. However, the increase of the mode volume with the increase in the BTJ mesa area results in the fall of the D-factor and the MCEF-factor (to $\sim 2.8-3.0$ GHz/mA$^{0.5}$ and $\sim 3.0-3.2$ GHz/mA$^{0.5}$ at the BTJ mesa diameter of 8 μm, correspondingly). As a result, there is no substantial improvement of the modulation characteristics of the studied WF-VCSELs with the increase in the BTJ mesa size.

Taking into account switching into the multi-mode lasing at the diameter of > 8 μm and the drop of the MCEF-factor with the increase in the BTJ mesa size, the biggest practical interest is in the single-mode lasers with the BTJ diameter of 6 μm. For them, the analysis of the rate and the range of data transmission of the studied VCSELs in the mode of direct current modulation has been performed with coding by the amplitude forma in the NRZ-mode using the pseudorandom binary sequence (PRBS) of the length (2^7-1) at the temperature of 20°C. The measurements were performed directly on the WF-VCSEL wafer without

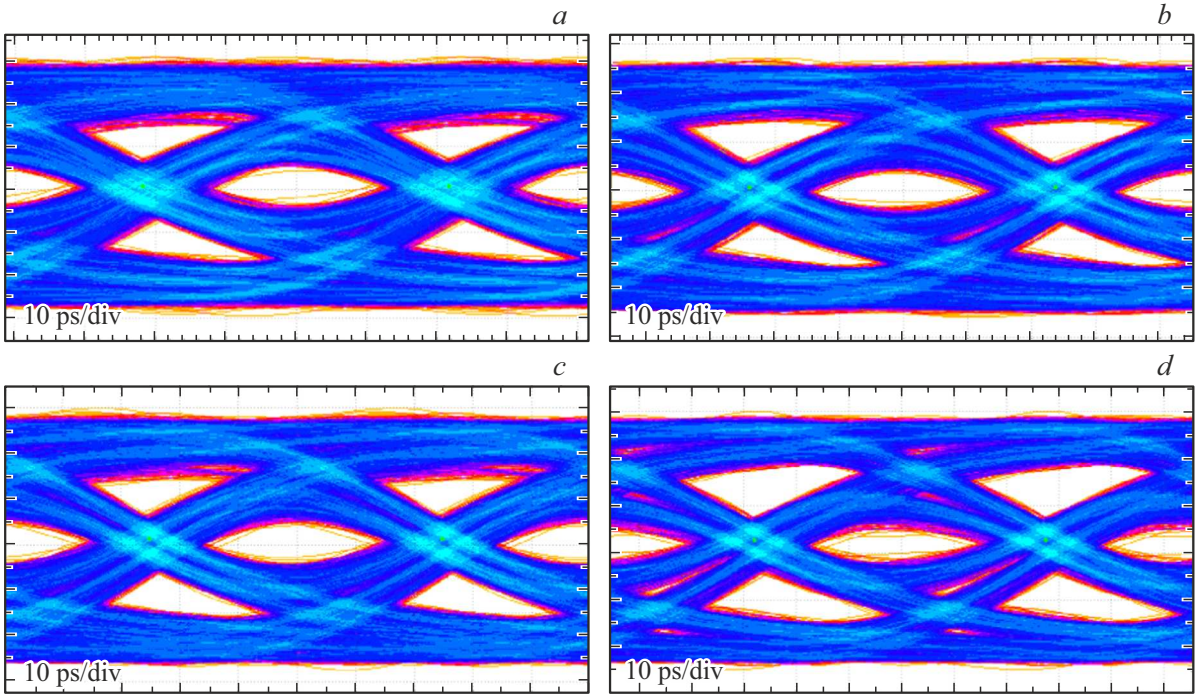

Figure 5. Eye diagrams of WF-VCSELs with the BTJ diameter of 6 μm at the direct current modulation in the NRZ-mode at the various length of the fiber-optic line: *a*) 23 Gb/s — the data transmission in the BTB configuration, *b*) 21 Gb/s — the data transmission for 500 m, *c*) 20 Gb/s — the data transmission for 1000 m, *d*) 18 Gb/s — the data transmission for 2000 m. The operating current — 16 mA, the modulating voltage — 300 mV. The measurement temperature — 20°C.

separating it into separate chips and mounting them into the HF casings. The initial modulating signal was formed by the binary combination generator SHF 12105A, and its amplitude was controlled by means of amplifiers and attenuators. Using the bias-tee, the modulating signal was added to the constant component giving a current operating point and then supplied to the laser by means of the HF probe. The WF-VCSEL radiation was introduced into the single-mode fiber SMF-28. The re-reflections were suppressed by an optical isolator. The optical sensor Tektronix DPO7OE1 with the bandpass of 33 GHz was used for transformation of the optical signal into the electric one, which was then record by the real-time oscillograph Tektronix DPO75902SX with the analogue bandwidth 59 GHz.

Fig. 5 shows the eye diagrams for a various length of the fiber-optic line. The operating current and voltage of the modulating digital signal were selected so as to ensure the maximum modulation bandwidth within the wide current range (i.e. simultaneously increase the data transmission rate and the height of eye diagram opening) and were $\sim$ 16 mA and 300 mV, respectively. The maximum transmission rate in the NRZ-mode for the BTB configuration is 23 Gb/s.The area of transition between the two adjacent clock interval (which corresponds to intersection of rising and falling fronts of the two eye diagrams) distinctly traces two separate groups of the front and fall lines, thereby indicating the presence of determined noise in the optical channel. At the same time, the blurred lines in each group indicate the presence of random noise.

We think that the source of the determined noise is related to the inter-symbol interference, which occurs in case of limitation of the traffic-carrying capacity of any component of the implemented optical communication line (a transmitter, a receiver, the transmission physical medium) and/or the reflection of the electric signal at the non-optimal match of the laser impedance with the signal generator (mismatch of the design of the UHF probe with the topology of the contact areas, the cutoff frequency of the laser equivalent diagram, etc.). It should be noted that it is difficult to localize and interpret the last mechanism. But, if the optical communication line has a problem of reflection of the electrical signal, then as a rule there is a problem of traffic-carrying capacity, too. Taking into account the results of the low-signal frequency analysis, then the key cause of inter-symbol interference is a relatively low cutoff parasitic frequency of the studied WF-VCSELs, which finally leads to amplitude variation of the optical signal at the high data communication rates depending on the length of repeated bits and previous bit states. As a result of the mismatch of the rising and falling time within the transition area of the eye diagram, the total jitter including the determined and random components reaches 23 ps, thereby corresponding to 53% of the clock signal ($\sim$ 0.31 UI). With increase in the length of the single-mode fiber, there is further increase in the jitter and decrease in the eye diagram opening

due to fiber dispersion, thereby finally resulting in the fall from the height of eye diagram opening. As a result, the described effect has limited the maximum rate of optical data transmission via the single-mode fiber at the value 21, 20 and 18 Gb/s for the line length 500, 1000 and 2000 meters, respectively.

4. Conclusion

It represents the results of the complex studies of the 1550 nm-range WF-VCSELs with the composite n^+-InGaAs/p^+-InGaAs/p^+-InAlGaAs BTJ and the active region based on the strained InGaAs/InGaAlAs quantum wells. It has demonstrated a general producibility of the lasing in the continuous lasing mode at 20°C with the threshold current < 2 mA and the slope efficiency > 0.4 W/A. The maximum output optical power in the single-mode lasing with the side mode suppression ratio > 40 dB exceeds 4.5 mW at 20°C. In accordance with the low-signal frequency analysis, the high-speed performance of the lasers is predominantly limited by the low cutoff parasitic frequency, which in the conditions of noticeable dumping results in the sharp decrease in the amplitude of the resonance peak at the moderate pumping currents. As a result, the modulation bandwidth is limited by 8 GHz at 20°C.

The analysis of the rate and the range of data transmission via the single-mode fiber in the mode of direct current modulation has been performed for the realized WF-VCSELs with the BTJ size of 6 μm with coding by the amplitude non-return-to-zero format. With the increase in the data transmission rate, there is the increase in the determined jitter predominantly due to inter-symbol interference, thereby limiting the opening of the eye diagram. With the increase in the length of the optical communication line, the fiber dispersion results in the amplification of this negative effect. As a result, the maximum rate of data transmission via the short optical communication line is 23 Gb/s, and when increasing the length of the optical communication line to 2000 m it drops to 18 Gbit/s.

The further improvement of the operating WF-VCSEL characteristics is associated with the increase in the temperature stability of the effective frequency of modulation. To solve first problem, it is required not only suppress the thermal escape of the carriers from the quantum well by applying more wide-band barriers, but to suppress the effect of saturating absorber by optimizing the depth of etching of the composite TJ (it requires a compromise with the high output optical power) and (or) increasing the spectrum mismatch of the spectrum in amplification of the active region in relation to the resonance wavelength (it requires a compromise with the low threshold current and the laser temperature stability). The solution of the second problem is related not only to reducing the parasitic capacitance of the reverse shifted p^+n-transition by reducing the doping level of the burial layer n-InP (it requires a compromise with a relatively low resistance of the laser) and minimization of the sizes of the device topology (it requires a compromise with the effective heat removal), but by reducing the mode volume (it requires the compromise with the high optical power), optimization of the lifetime of th photons (it requires the compromise with the low threshold current) and the increase in the differential gain of the active region (it requires the compromise with thermal escape of the carriers).

Funding

The study has been performed by a group of authors from ITMO University and financed by the program „Priority 2030“ in terms of studies of the number of the dynamic characteristics, as well as with the support of the Ministry of Science and Higher Education of the Russian Federation, the research project No. 2019−1442 in terms of a number of studies of the static characteristics.

Conflict of interest

The authors declare that they have no conflict of interest.

References

[1] *VCSEL Industry: Communication and Sensing, The ComSoc Guides to Communications Technologies,* ed. by B.D. Padullaparthi, J. Tatum, K. Iga (Wiley-IEEE Press, Piscataway, N.J., USA, 2022). ISBN: 978-1-119-78221-6
[2] L. Zhang, J. Chen, E. Agrell, R. Lin, L. Wosinska. J. Lightwave Technol., **38** (1), 18 (2020). DOI: 10.1109/JLT.2019.2941765
[3] A. Larsson, P. Westbergh, J.S. Gustavsson, E. Haglund, E.P. Haglund. In: Proc. SPIE OPTO (San Francisco, CA, USA, Mar. 2015) v. 9381, p. 93810D-1. DOI: 10.1117/12.2082614
[4] L. Zhang, J. Van Kerrebrouck, R. Lin, X. Pang, A. Udalcovs, O. Ozolins, S. Spiga, M.-C. Amann, G. Van Steenberge, L. Gan, M. Tang, S. Fu, R. Schatz, S. Popov, D. Liu, W. Tong, S. Xiao, G. Torfs, J. Chen, J. Bauwelinck, X. Yin. J. Lightwave Technol., **37** (2), 380 (2019). DOI: 10.1109/JLT.2018.2851746
[5] M.-R. Park, O.-K. Kwon, W.-S. Han, K.-H. Lee, S.-J. Park, B.-S. Yoo. IEEE Phot. Technol. Lett., **18** (16), 1717 (2006). DOI: 10.1109/LPT.2006.879940
[6] W. Hofmann, M. Müller, A. Nadtochiy, C. Meltzer, A. Mutig, G. Böhm, J. Rosskopf, D. Bimberg, M.-C. Amann, C. Chang-Hasnain. Opt. Express, **17** (20), 17547 (2009). DOI: 10.1364/OE.17.017547
[7] W. Hofmann. IEEE Photonics J., **2** (5), 802 (2010). DOI: 10.1109/JPHOT.2010.2055554
[8] S. Spiga, W. Soenen, A. Andrejew, D.M. Schoke, X. Yin, J. Bauwelinck, G. Boehm, M.-C. Amann. J. Lightwave Technol., **35** (4), 727 (2017). DOI: 10.1109/JLT.2016.2597870
[9] S. Spiga, D. Schoke, A. Andrejew, G. Boehm, M.-C. Amann. J. Lightwave Technol., **35** (15), 3130 (2017). DOI: 10.1109/jlt.2017.2660444
[10] A. Caliman, A. Mereuta, G. Suruceanu, V. Iakovlev, A. Sirbu, E. Kapon. Opt. Express, **19** (18), 16996 (2011). DOI: 10.1364/OE.19.016996

[11] A.V. Babichev, L.Y. Karachinsky, I.I. Novikov, A.G. Gladyshev, S.A. Blokhin, S. Mikhailov, V. Iakovlev, A. Sirbu, G. Stepniak, L. Chorchos, J.P. Turkiewicz, K.O. Voropaev, A.S. Ionov, M. Agustin, N.N. Ledentsov, A.Y. Egorov. IEEE J. Quant. Electron., **53** (6), 1 (2017). DOI: 10.1109/JQE.2017.2752700
[12] T. Grundl, P. Debernardi, M. Muller, C. Grasse, P. Ebert, K. Geiger, M. Ortsiefer, G. Bohm, R. Meyer, M.-C. Amann. IEEE J. Select. Top. Quant. Electron., **19** (4), 1700913. DOI: 10.1109/JSTQE.2013.2244572
[13] A. Sirbu, G. Suruceanu, V. Iakovlev, A. Mereuta, Z. Mickovic, A. Caliman, E. Kapon. IEEE Phot. Technol. Lett., **25** (16), 1555 (2013). DOI: 10.1109/LPT.2013.2271041
[14] D. Ellafi, V. Iakovlev, A. Sirbu, G. Suruceanu, Z. Mickovic, A. Caliman, A. Mereuta, E. Kapon. Opt. Express, **22** (26), 32180 (2014). DOI: 10.1364/OE.22.032180
[15] E.S. Kolodeznyi, S.S. Rochas, A.S. Kurochkin, A.V. Babichev, I.I. Novikov, A.G. Gladyshev, L.Ya. Karachinskii, D.V. Denisov, Yu.K. Bobretsova, A.A. Klimov, S.A. Blokhin, K.O. Voropaev, A.S. Ionov. Opt. Spectr., **125**, 238 (2018). DOI: 10.1134/S0030400X18080143
[16] C.A. Wang, B. Schwarz, D.F. Siriani, L.J. Missaggia, M.K. Connors, T.S. Mansuripur, D.R. Calawa, D. Mc Nulty, M. Nickerson, J.P. Donnelly, K. Creedon, F. Capasso. IEEE J. Select. Top. Quant. Electron., **23** (6), Art no. 1200413 (2017). DOI: 10.1109/JSTQE.2017.2677899
[17] S.A. Blokhin, M.A. Bobrov, N.A. Maleev, A.A. Blokhin, A.G. Kuz'menkov, A.P. Vasil'ev, S.S. Rochas, A.G. Gladyshev, A.V. Babichev, I.I. Novikov, L.Ya. Karachinsky, D.V. Denisov, K.O. Voropaev, A.S. Ionov, A.Yu. Egorov, V.M. Ustinov. Techn. Phys. Lett., **46** (17), 854 (2020). DOI: 10.1134/S1063785020090023
[18] S.A. Blokhin, A.V. Babichev, A.G. Gladyshev, L.Ya. Karachinsky, I.I. Novikov, A.A. Blokhin, S.S. Rochas, D.V. Denisov, K.O. Voropaev, A.S. Ionov, N.N. Ledentsov, A.Yu. Egorov. Electron. Lett., **57** (18), 697 (2021). DOI: 10.1049/ell2.12232
[19] S.A. Blokhin, A.V. Babichev, A.G. Gladyshev, L.Ya. Karachinsky, I.I. Novikov, A.A. Blokhin, M.A. Bobrov, N.A. Maleev, V.V. Andryushkin, D.V. Denisov, K.O. Voropaev, I.O. Zhumaeva, V.M. Ustinov, A.Yu. Egorov, N.N. Ledentsov. IEEE J. Quant. Electron., **58** (2), Art № 2400115 (2022). DOI: 10.1109/JQE.2022.3141418
[20] S.A. Blokhin, V.N. Nevedomsky, M.A. Bobrov, N.A. Maleev, A.A. Blokhin, A.G. Kuzmenkov, A.P. Vasyl'ev, S.S. Rohas, A.V. Babichev, A.G. Gladyshev, I.I. Novikov, L.Ya. Karachinsky, D.V. Denisov, K.O. Voropaev, A.S. Ionov, A.Yu. Egorov, V.M. Ustinov. Semiconductors, **54** (10), 1276 (2020). DOI: 10.1134/S1063782620100048
[21] M. Ortsiefer, R. Shau, G. Böhm, F. Köhler. M.-C. Amann. Appl. Phys. Lett., **76** (16), 2179 (2000). DOI: 10.1063/1.126290
[22] S.A. Blokhin, M.A. Bobrov, A.A. Blokhin, N.A. Maleev, A.G. Kuz'menkov, A.P. Vasil'ev, S.S. Rochas, A.V. Babichev, I.I. Novikov, L.Ya. Karachinskiy, A.G. Gladyshev, D.V. Denisov, K.O. Voropaev, A.Yu. Egorov, V.M. Ustinov. Pis'ma ZhTF, **47** (22), 3 (2021) (in Russian).
[23] K.O. Voropaev, B.I. Seleznev, A.Yu. Prokhorov, A.S. Ionov, S.A. Blokhin. J. Phys.: Conf. Ser., **1658**, 012069 (2020). DOI: 10.1088/1742-6596/1658/1/012069
[24] J. Bengtsson, J. Gustavsson, Å. Haglund, A. Larsson, A. Bachmann, K. Kashani-Shirazi, V.-C. Amann. Opt. Express, **16** (25), 20789 (2008). DOI: 10.1364/OE.16.020789
[25] S.A. Blokhin, M.A. Bobrov, A.A. Blokhin, A.G. Kuz'menkov, A.P. Vasil'ev, N.A. Maleev, S.S. Rochas, A.G. Gladyshev, A.V. Babichev, I.I. Novikov, L.Ya. Karachinskiy, D.V. Denisov, K.O. Voropaev, A.S. Ionov, A.Yu. Egorov, V.M. Ustinov. Pis'ma ZhTF, **46** (24), 49 (2020) (in Russian).
[26] V.V. Lysak, K.S. Chang, Y.T. Lee. Appl. Phys. Lett., **87** (23), Art. № 231118 (2003). DOI: 10.1063/1.2140886
[27] *VCSELs: Fundamentals, Technology and Applications of Vertical-Cavity Surface-Emitting Lasers*. Springer Series in Optical Sciences, ed. by R. Michalzik (Springer, Berlin–Heidelberg, 2013). DOI: 10.1007/978-3-642-24986-0